Advances in Engineering Software 130 (2019) 1–13

Contents lists available at ScienceDirect

Advances in Engineering Software

journal homepage: www.elsevier.com/locate/advengsoft

The AMORE paradigm for finite element analysis☆

Klaus-Jürgen Bathe

Massachusetts Institute of Technology, Cambridge, MA 02139, USA

ARTICLE INFO

Keywords:
Meshing
Computer-aided design and engineering
Finite element analysis
Overlapping finite elements
Static and dynamic solutions
Wave propagations

ABSTRACT

The objective in this paper is to largely review, but also give new insight into, the recent development of a novel paradigm for finite element analysis. The approach enables much easier meshing than usually performed for finite element analysis and then the computationally efficient solution of the finite element model. The important aspects of the paradigm are the automatic meshing on any given geometry (typically given by use of a CAD program or a computerized scan) with the use of overlapping and regular finite elements – hence the acronym AMORE for Automatic Meshing with Overlapping and Regular Elements. We summarize the basic steps used in the paradigm, give the basic equations to formulate the overlapping elements, discuss specific attributes, give some applications and conjecture on the further development and use of the solution scheme. Our discussion is based on previously published work with a focus on simplifying the formulation of the overlapping elements, providing novel insight, and suggesting a notation. The paradigm has so far only been applied in the linear analyses of solids, however embodies significant potential for general and wide use in computer-aided engineering.

1. Introduction

Finite element analyses are now abundantly performed for engineering designs and in scientific studies. For such analyses, in computer-aided engineering (CAD), a program may be used to generate the geometry, which is "cleaned up", and then a finite element mesh is spanned [1]. Alternatively, another description of the geometry, as for example obtained from a three-dimensional (3D) computerized scan in the medical and building industries, may be used and meshed. Much attention has been focused on the effort of meshing in order to render the process highly automatic. Various meshing programs have been developed and are offered as stand-alone tools, like HyperMesh and Gmsh [2,3], or as part of widely-used finite element analysis programs, like ANSYS, SIMULIA, NX Siemens, and ADINA.

However, while much effort has been expended to obtain efficient meshing programs for finite element analysis, there are still difficulties to reach, in general, effective meshes for a specific analysis. For this reason, meshless methods have been proposed for many applications, see for example [4–7] and the isogeometric analysis approach has been abundantly researched, see for example [8–10]. Meshless procedures require little computational effort to discretize the continuum, however, the numerical integration in a reliable procedure to obtain the governing equations is computationally very expensive, often prohibitively so. Hence these schemes are hardly used in engineering practice. The isogeometric analysis approach has been researched to enable more effective finite element analysis when a specific CAD geometry is given. In this approach the specific CAD functions used for establishing the geometry are also employed to formulate the finite element governing equations.

Our experience in finite element analysis is that low-order elements are widely preferred, and widely used, specifically the 4-node quadrilateral elements for two-dimensional (2D) solutions and corresponding 8-node elements for 3D solutions. The highest-order elements widely used are probably the 10- and 11-node tetrahedral elements for 3D analyses. These elements are direct extensions of the too stiff 4-node tetrahedral element used efficiently in 3D free form meshing.

We have focused on the development of a novel meshing approach with the use of mostly undistorted low-order regular, traditional elements and the use of overlapping elements [11–16]. The reason for using "overlapping elements" is that highly distorted overlapping elements can be employed efficiently. Therefore, it is possible to mesh much of the geometry in an effective manner with traditional finite elements of undistorted geometry (for which these elements show best performance [1]) and use only in some regions the overlapping elements. This is the premise of the AMORE paradigm, using Automatic Meshing with Overlapping and Regular Elements.

☆ This paper focuses on part of the author's plenary presentation at the Conferences "Computational Engineering Technology" and "Computational Structures Technology", Sitges, Barcelona, Spain, Sep. 2018.

E-mail address: kjb@mit.edu.

https://doi.org/10.1016/j.advengsoft.2018.11.010
Received 11 October 2018; Received in revised form 23 November 2018; Accepted 29 November 2018
Available online 15 February 2019
0965-9978/

Of course, overlapping grids have been used for some time in CFD solutions, like in chimera overset-grid schemes [17–20]. However, in those solutions, distinct grids of finite volumes or finite differences are separately generated and then overlaid to cover the complete continuum. The approach is like gluing grids together over parts of their surfaces, with a gluing algorithm. The use of the AMORE scheme in finite element analysis is quite different and offers much more generality.

Our objective in this paper is to describe the AMORE paradigm, give the formulations of some overlapping finite elements with novel insights in the solution scheme, and suggest a notation to be used in further research. We present some illustrative applications and conjecture that we see the paradigm as a powerful procedure for general finite element analyses of solids, shells, fluids and multi-physics problems. However, there are many outstanding research tasks that need to be tackled first to render the solution scheme very general and widely applicable.

We focus on a summary of the paradigm with new insights. Hence the paper is largely a review paper specific to the paradigm we have worked on and we draw considerably on the material already presented in Refs. [12–16].

2. The AMORE paradigm

The AMORE scheme is given by the following algorithmic steps:

Step 1: A mesh of cells is spanned over the geometry to be analyzed; hence the geometry is immersed in a mesh, usually a Cartesian mesh but it could be a curvilinear mesh as well. In 3D analysis, the sides of a cell are of lengths Δx, Δy, Δz. Unless the sides are constant in lengths and for a rectangle/ brick, the cells are geometrically distorted. Since in finite element analysis, undistorted elements are most effective, it is frequently best to use rectangular cells of constant Δx, Δy, Δz. However, in practice, local mesh refinements may then be needed.

We emphasize that the geometry to be analyzed could be the output from any CAD program or been obtained by any other means, like from a 3D computerized scan.

Step 2: The boundary of the geometry is meshed. In 2D analyses, the boundary lines are meshed using two-node straight lines, and in 3D analyses, the boundary surfaces are meshed using 3-node triangular flat facets. In some geometry descriptions, two-node lines and triangular facets are already used to define the geometry and hence do not need to be created in this step. The lines and facets can vary in size and are automatically adjusted in size to accurately capture the geometry. The sizes of lines and facets are independent of the values Δx, Δy, Δz and are generated to "neglect or span over" deficiencies in the geometry description, when present, like gaps that provide a non-water tight geometry. This boundary representation represents a "cleaning-up" of the geometry and is an important ingredient, which in practice should be programmed to be automatic but also be available for the analyst to steer. Algorithms for this step are largely available but could be improved.

A key is here that a mesh of lower dimension is spanned eliminating geometry defects and the 'entities' in that mesh can be quite distorted and in size independent of the values of Δx, Δy, Δz (used for the Cartesian mesh) because the overlapping finite elements employed in the next steps are quite distortion-insensitive.

Step 3: All cells of the Cartesian mesh spanned in step 1 that lie outside the discretized boundary of the geometry or cut that boundary are removed. The remaining cells are converted into low-order regular finite elements. The result is that there are regions of the discretized geometry which are not covered by finite elements.

Step 4: The empty regions obtained in Step 3 are filled in with overlapping and coupling finite elements. The ideal case of using overlapping elements in the AMORE paradigm is schematically depicted in Fig. 1 where disks and undistorted quadrilateral elements in 2D analyses (spheres and brick elements in 3D analyses) are

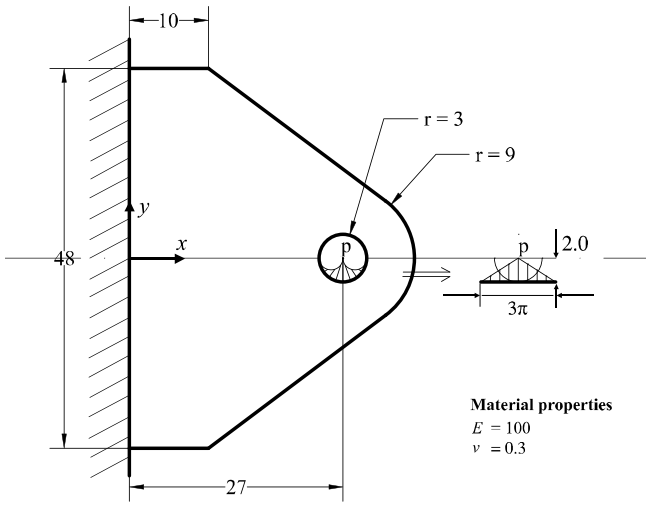

(a)

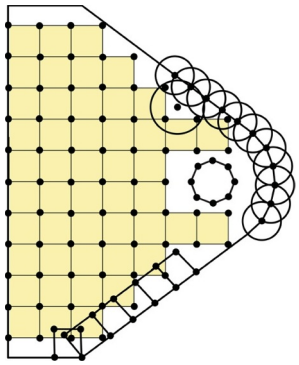

(b)

Fig. 1. AMORE schematically for the analysis of a bracket; (a) geometry; (b) mesh used showing only some overlapping elements.

overlapping [11]. However, to achieve this generality requires further research to reach a computationally efficient scheme.

A more direct and geometrically simpler way to proceed is shown in Fig. 2 where, for the 2D analysis, we use for the uncovered regions simply a triangular grid [12]. Here the overlapping elements are polygonal elements that are geometrically not identified in the figure but that overlap to form the interpolation functions for the triangular elements shown in the figure. As we discuss below, the nodes of the triangular elements are used as the centers of disks (tetrahedral elements and spheres in 3D analyses). The key is that the simple triangular finite elements can be highly distorted without losing their predictive capabilities. The same property holds for quadrilateral elements and in 3D analyses for tetrahedral and brick elements. Hence an efficient meshing using these elements can be performed.

Figs. 3–5 show the steps of analysis using the AMORE scheme for the geometry obtained using a computer-aided design program. The geometry pertains to a cantilever with holes. We note that a Cartesian grid is spanned to contain the complete geometry of the structure, that the boundary of the geometry is discretized with the removal of geometry defects, that the cells not entirely inside the boundary discretization are removed (additional cells are also removed to enable the placing of coupling elements), that the remaining cells are turned into regular finite elements, and that the empty space is filled with overlapping and coupling finite elements. We discuss the stress solution results in Section 4.1.

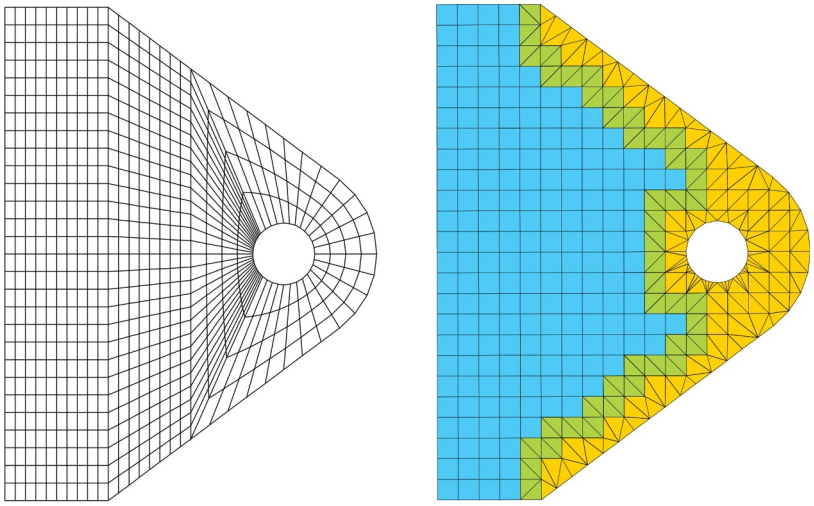

(a) Traditional mesh (b) AMORE mesh

Fig. 2. AMORE used in the problem of Fig. 1, using triangular basic elements for the overlapping polygonal elements.

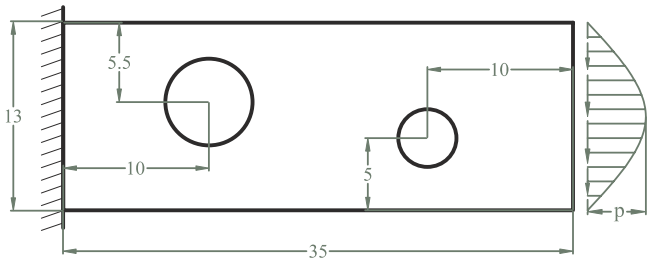

Fig. 3. Cantilever plate in plane stress conditions ($E = 200 \times 10^9, \nu = 0.3$, thickness = 1.0), radii of holes = 2 and 3; quadratic tangential traction; $p = 1000$.

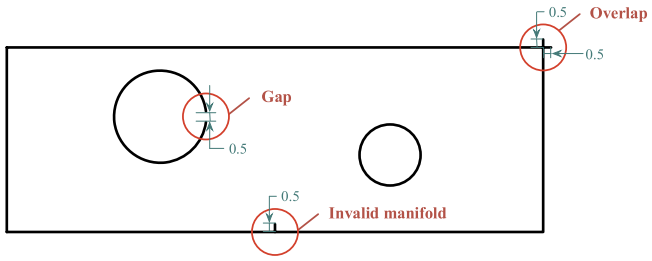

Fig. 4. A CAD representation of the cantilever plate; three geometrical imperfections.

The geometry in this example solution is based on using a CAD program; however, for the AMORE scheme the geometry could, for example, also have been obtained from a computerized scan.

While we focus in this paper on the overlapping elements and coupling schemes used in Fig. 2, the basic concepts are also applicable to formulating other overlapping elements; however, such formulations may require more research.

3. Formulation of overlapping and coupling elements

In this section we give the formulation of the finite elements that we so far used in the AMORE scheme. The regular (or traditional) elements are those used widely and we need to only recall that these elements are optimal in their performance when geometrically undistorted [1]. Hence we only need to focus on the formulation of the overlapping finite elements and their coupling to the regular elements.

3.1. The overlapping elements

For clarity of exposition, we consider the 2D analyses of solids and show figures for that case, but the equations can be directly extended for the analysis of 3D problems [14].

In principle, for 2D analyses, the use of 3-node triangular elements is quite natural but these elements can hardly be used efficiently in certain practical analyses because they are too stiff to solve bending-dominated problems. Instead, the use of 4-node quadrilateral elements is preferred but even these elements should not be geometrically distorted [1]. In the text below, we describe first in detail new 3-node triangular elements that are given by the overlapped regions of overlapping polygonal elements. The same concepts can be used for the formulation of new 4-node quadrilateral elements, and the corresponding 3D elements.

The overlapping element formulation given below embodies some basic and key concepts:

- We focus on a grid of nodes generated over the domain to be analyzed using the overlapping finite elements. Considering the 3-node element, the grid represents the analysis domain as a collection of 3-node triangular finite elements.
- The new 3-node finite elements are obtained from the “overlapped regions” of polygonal elements.
- To construct the interpolation functions for the triangular 3-node elements, we place spheres of suitable radii, here disks in 2D analysis, like in the method of finite spheres [5], at each of the nodes of the 3-node elements; each disk “carries” its Shepard function.
- With the placing of the spheres, each node carries polynomial (or other suitable) nodal degrees of freedom like in the method of finite spheres.
- We interpolate in an effective manner, using polynomials, the Shepard function of each sphere. This interpolation is important to only have polynomials to integrate for the element stiffness and mass matrices.
- The spheres of the nodes interact, because they overlap in the region of the 3-node triangular element.
- We interpolate the nodal contributions linearly over the 3-node triangular element, like in the traditional finite element solution.
- The final interpolation functions over each 3-node triangular element provide a compatible displacement field over the complete domain.

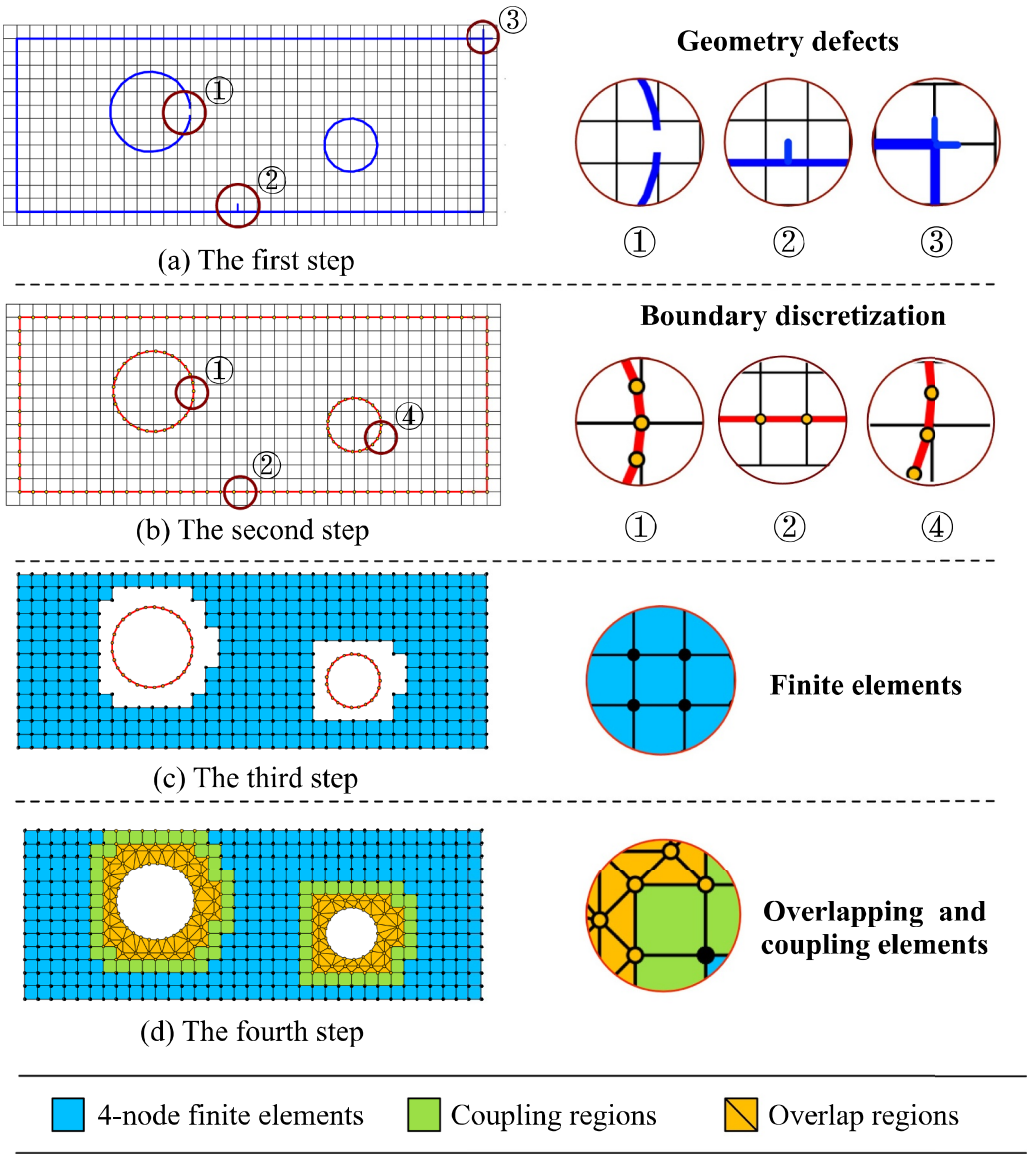

Fig. 5. The steps using AMORE; (a) the generated Cartesian grid, geometry defects: ① gap, ② invalid manifold, ③ overlap; (b) straight line Δs- segmentation of the boundary, the geometry defects are removed, ① Δs_1- segmentation, ② Δs_2- segmentation, ④ Δs_3- segmentation; (c) internal cells retained and converted to 4-node regular finite elements; (d) overlapping and coupling finite elements are used to fill empty space.

- To form the governing element stiffness and mass matrices of the element assemblage we only integrate contributions over each of the 3-node triangular elements, just like in traditional finite element analysis.

The same basic and key concepts apply also to the formulation of general 4-node quadrilateral elements. Of course, then a grid of 4-node elements, instead of 3-node elements, is used to span the geometry to be analyzed. In a similar manner the formulation of 3D elements is tackled.

The above procedure renders the formulation effective because, firstly, the predictive capability of the triangular element is distortion-insensitive, secondly, only polynomials are used in the formulation enabling efficient numerical integration, and thirdly, the bandwidth given by *nodal* interactions is as in traditional finite element analysis. Of course, the actual bandwidth is, in addition, given by the degrees of freedom at each node.

3.1.1. *Triangular elements from the overlapping of polygonal elements*

Consider the triangulated region in Fig. 6. For node *I*, we consider the five triangular 3-node elements coupling into that node to make up the 6-node polygonal element. For node *L*, we have six 3-node elements to make up a 7-node polygonal element, and for node *M*, we have seven 3-node elements to make up an 8-node polygonal element. Each node in this mesh is therefore the center node of a polygonal element of more than 3 nodes. In Fig. 6, the polygonal elements with center nodes *I, L* and *M* overlap on the basic 3-node element *I-L-M*.

The interpolation used for the overlap region *I-L-M* (the 3-node element) is given by

$$\mathbf{u}(\mathbf{x}) = h_I \psi_I(\mathbf{x}) + h_L \psi_L(\mathbf{x}) + h_M \psi_M(\mathbf{x}) \tag{1}$$

where the h_I, h_L, h_M are the usual finite element interpolation functions of the traditional 3-node element. Note that the interpolation in Eq. (1) provides for continuity of the displacement field over the complete analysis domain by an appropriate choice of ψ_I, ψ_L, ψ_M.

We identify the region *I-L-M* as a 3-node element given by the *overlapping of the three polygonal elements* with center nodes *I, L* and *M*, see Fig. 6. The aim is to establish functions ψ_I, ψ_L, ψ_M that are continuous over the 3-node elements, from element to element, that render the 3-node element *I-L-M* effective for stress predictions *and* render it distortion-insensitive. The key for this element behavior is to have

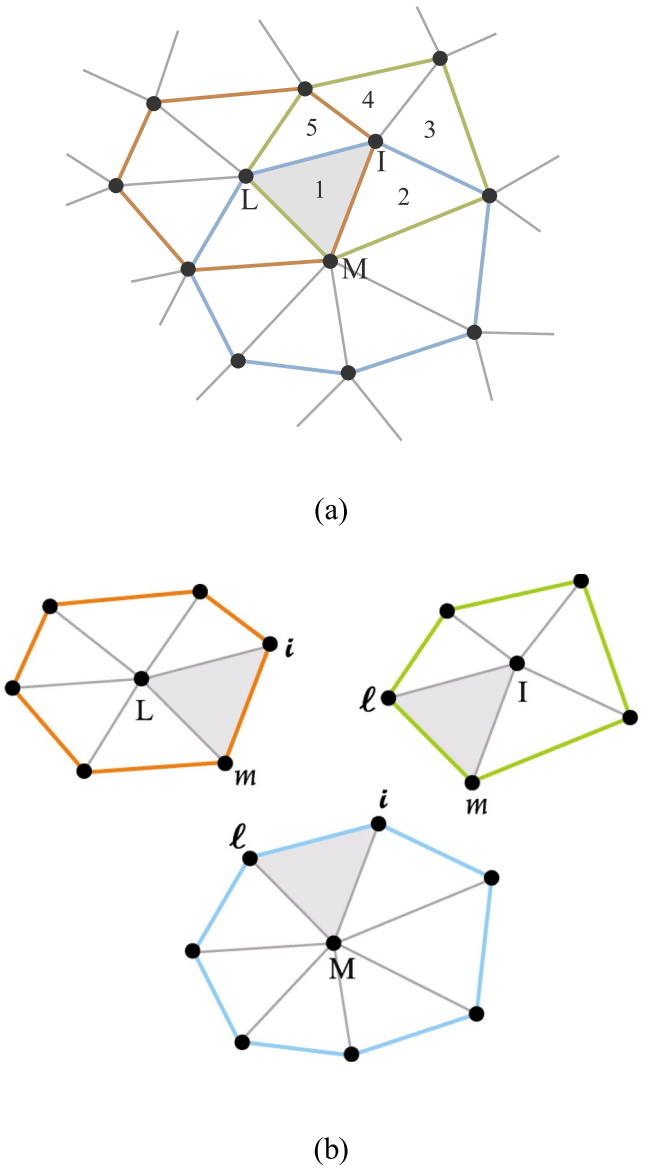

Fig. 6. Triangularization and overlapping elements; (a) triangularization; (b) overlapping elements, the overlap region is shaded, capital letters denote the centers of the polygonal elements.

nodes *L* and *M* influence the interpolation established for node *I*, similarly for nodes *L* and *M*, and associate with each node *I, L,* and *M* not just a single degree of freedom but a polynomial or other function, like in the finite element method using covers [21].

Let us assume that we have identified a weight function $\phi_J^I(x)$ which "gives a weight from node *J* to node *I*", then we can write

$$\psi_I(\mathbf{x}) = \sum_{J=I,L,M} \phi_J^I \mathbf{u}_J \tag{2a}$$

with the $\mathbf{u}_J$ degrees of freedom given by the coefficients $\mathbf{a}_{Jn}$ in

$$\mathbf{u}_J = p_n \mathbf{a}_{Jn} \tag{2b}$$

where we imply the summation convention over the index n . Assuming only polynomial terms are used, p_n denotes the nth polynomial term in the vector

$$\mathbf{p}^T = [1 \quad x \quad y \quad x^2 \quad xy \quad \ldots] \tag{3}$$

where *(x,y)* corresponds to a local coordinate system at node *J*, and we non-dimensionalize the terms (using suitable length factors) in order to

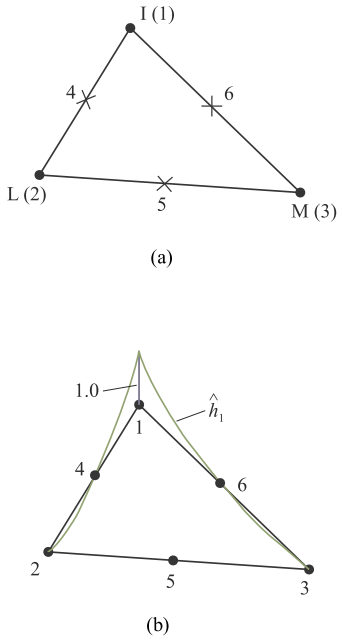

Fig. 7. Interpolation over the overlap domain; (a) physical nodes I, L, M (or 1, 2, 3) and fictitious nodes 4, 5, 6 for the overlap region; (b) traditional interpolation function of 6-node element corresponding to node 1.

prevent ill-conditioning of the governing finite element equilibrium equations.

We note that in Eq. (2a) the $\mathbf{u}_J$ are the degrees of freedom at node *J* and in Eq. (2b) these are then given by the $\mathbf{a}_{Jn}$. Hence, in general, the degrees of freedom correspond to the terms in the polynomial of Eq. (3) and if in Eq. (3) only the constant term (= 1) is used we have only the traditional degrees of freedom at the node.

While not chosen yet, we recognize that for an effective solution, ϕ_J^I should involve *only* polynomials over the overlap region (like in traditional finite element analysis) and interpolate the weight function to have stability and good accuracy. To this aim, we introduce additional mid-side "fictitious" nodes on the domain *I-L-M,* see Fig. 7, and use the shape functions $\hat{h}_i$ of the traditional 6-node element

$$\phi_J^I = \sum_{i=1}^{6} \hat{h}_i \hat{\phi}_{Ji}^I \tag{4}$$

where $\hat{\phi}_{Ji}^I$ is the "nodal value at node *i*" of the weight function used. It is important to note that there are no nodal displacement degrees of freedom at the fictitious mid-side nodes and that these nodes are only used to interpolate the weight function.

Hence we finally have for the 3-node triangular element *I-L-M*

$$\psi_I(\mathbf{x}) = \sum_{J=I,L,M} \hat{h}_i \hat{\phi}_{Ji}^I \mathbf{u}_J \tag{5}$$

where the summation over *i* is implied.

Similarly we also have

$$\psi_L(\mathbf{x}) = \sum_{J=I,L,M} \hat{h}_i \hat{\phi}_{Ji}^L \mathbf{u}_J \tag{6}$$

$$\psi_M(\mathbf{x}) = \sum_{J=I,L,M} \hat{h}_i \hat{\phi}_{Ji}^M \mathbf{u}_J \tag{7}$$

Hence $\mathbf{u}(\mathbf{x})$ for the 3-node element (the domain overlapped by the 3 polygonal elements, see Fig. 6) is thus given by Eq. (1).

An important ingredient in the formulation is the weight function used. We have various choices for a weight function and it is still an open question which function is optimal. So far we have employed the Shepard function like used in the method of finite spheres and

Table 1
Nodal values used for the quadratic interpolation of the Shepard functions with centers at nodes I = 1, L = 2, M = 3. The node numbering is given in Fig. 7.

Nodes	1	2	3	4	5	6
$\hat{\phi}^1_{1i}$	1	0	0	$\frac{W_1}{W_1+W_2}\vert_{X_4}$	$\frac{W_1}{W_1+W_2+W_3}\vert_{X_5}$	$\frac{W_1}{W_1+W_3}\vert_{X_6}$
$\hat{\phi}^1_{2i}$	0	1	0	$\frac{W_2}{W_1+W_2}\vert_{X_4}$	$\frac{W_2}{W_1+W_2+W_3}\vert_{X_5}$	0
$\hat{\phi}^1_{3i}$	0	0	1	0	$\frac{W_3}{W_1+W_2+W_3}\vert_{X_5}$	$\frac{W_3}{W_1+W_3}\vert_{X_6}$
(a) For ψ_I						
Nodes	1	2	3	4	5	6
$\hat{\phi}^2_{1i}$	1	0	0	$\frac{W_1}{W_1+W_2}\vert_{X_4}$	0	$\frac{W_1}{W_1+W_2+W_3}\vert_{X_6}$
$\hat{\phi}^2_{2i}$	0	1	0	$\frac{W_2}{W_1+W_2}\vert_{X_4}$	$\frac{W_2}{W_2+W_3}\vert_{X_5}$	$\frac{W_2}{W_1+W_2+W_3}\vert_{X_6}$
$\hat{\phi}^2_{3i}$	0	0	1	0	$\frac{W_3}{W_2+W_3}\vert_{X_5}$	$\frac{W_3}{W_1+W_2+W_3}\vert_{X_6}$
(b) For ψ_L						
Nodes	1	2	3	4	5	6
$\hat{\phi}^3_{1i}$	1	0	0	$\frac{W_1}{W_1+W_2+W_3}\vert_{X_4}$	0	$\frac{W_1}{W_1+W_3}\vert_{X_6}$
$\hat{\phi}^3_{2i}$	0	1	0	$\frac{W_2}{W_1+W_2+W_3}\vert_{X_4}$	$\frac{W_2}{W_2+W_3}\vert_{X_5}$	0
$\hat{\phi}^3_{3i}$	0	0	1	$\frac{W_3}{W_1+W_2+W_3}\vert_{X_4}$	$\frac{W_3}{W_2+W_3}\vert_{X_5}$	$\frac{W_3}{W_1+W_3}\vert_{X_6}$
(c) For ψ_M						

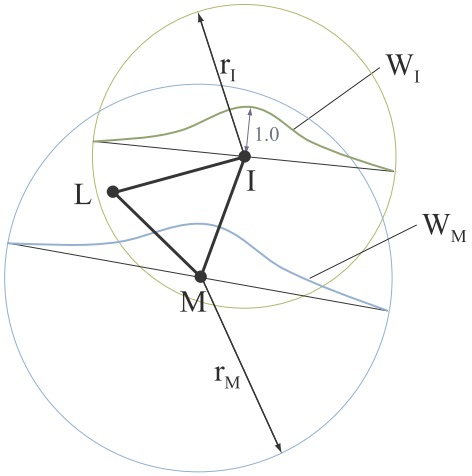

Fig. 8. Weight functions for nodes I and M (shown schematically).

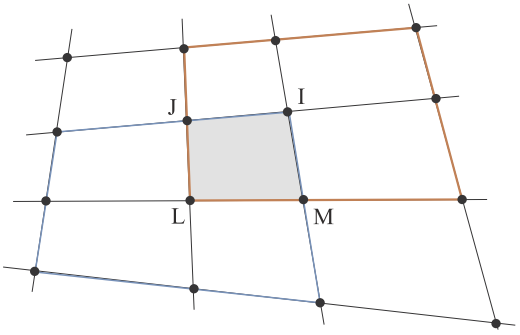

Fig. 9. Four 9-noded straight-sided polygonal elements overlap on region I-J-L-M. Each 9-node element consists of four 4-node elements.

interpolate the function using the values given in Table 1,

$$\hat{\phi}^I_{Ji}(\mathbf{x}) = \frac{W_J(\mathbf{x})}{\sum_K W_K(\mathbf{x})}\bigg|_{\text{at position } i,\ X_i} \tag{8}$$

where the summation is over the appropriate K (discussed below, see Table 1), W_J is a weight function for node J and is chosen to be, see Fig. 8,

$$W_J(\mathbf{x}) = \begin{cases} 1 - 6s^2 + 8s^3 - 3s^4 & (0 \le s \le 1) \\ 0 & (s > 1) \end{cases} \tag{9}$$

with s given by

$$s = \frac{d_J}{\alpha r_J} \tag{10}$$

where d_J denotes the distance between node J and point $\mathbf{x}=(x, y)$, r_J is a chosen radius for node J selected to contain the polygonal element corresponding to node J and α is a constant. We choose r_J to be just large enough to have the circle contain the complete polygonal element. The solution will depend on the value of α, for example, as αr_J becomes large and approaches infinity, the scheme reduces to the finite element method with interpolation covers [21], a method we found not as effective in the problems solved in Ref. [14]. However, for different elements and different problem solutions, the use of interpolation covers may be effective. In our solutions we used $\alpha = 1$, but more research is needed to establish rules for an "overall optimal" value of α and possibly find other more effective weight functions.

Hence, in essence, we use disks, like in the method of finite spheres, at each of the three corner nodes of the triangular 3-node element, and each of the disks has the polynomial degrees of freedom given in Eqs. (2a), (2b), and (3). In Eq. (8), the superscript denotes for which traditional nodal interpolation the right-hand side is evaluated and the subscript J denotes the node (center) of the Shepard function.

Important requirements for the functions defined in Eqs. (5)–(7) are that the functions be continuous with the functions of the neighboring triangular elements and that the sum of the functions is equal to 1. If these requirements are fulfilled, the rigid body mode criterion is satisfied and the patch tests are passed (provided, of course, the nodal polynomial degrees of freedom contain the patch test functions to be represented). We satisfy these requirements for the following reasons.

Consider the element in Fig. 6 and the function $h_I\psi_I(\mathbf{x})$ for node I with Table 1. Compatibility over the sides I-L and I-M is provided because only the disks on nodes I and L for side I-L and nodes I and M for side I-M are used respectively. Compatibility over the side L-M is provided because the function h_I is zero on that edge. Further, we note that the functions for ψ_I with the nodal values given in Table 1(a) sum to 1.0. Analogous reasoning is used when considering nodes L and M. Hence compatibility is satisfied, the right-hand sides in Eqs. (5)–(7) with unit displacements sum each to 1, and since $h_I + h_L + h_M = 1$ and the polynomial degrees of freedom are used at the nodes, we satisfy all criteria for convergence of the overlapping finite element scheme.

We also see that since the functions $\psi_I(\mathbf{x})$, $\psi_L(\mathbf{x})$, $\psi_M(\mathbf{x})$ each contain the assumed polynomial of Eq. (3) as degrees of freedom (see Eqs. (5)–(7)), this polynomial can be represented irrespective of the geometric distortions of the 3-node element. It is for this reason that the 3-node element is distortion-insensitive, which is quite different from the behavior of the traditional higher-order finite elements [1]. However, while this property of the 3-node element is very valuable, of course, the solution results will somewhat change as the element geometry is changed because, simply, the polynomials used are then assumed to represent the solution over different spatial regions. We give some results in Section 4 and refer to Refs. [11–16].

To obtain insight into the interpolation used and a compact form, we expand Eq. (1) using the above relations to obtain, with the summation over the index i,

$$\begin{aligned} \mathbf{u}(\mathbf{x}) \;=\; & h_I\left(\hat{h}_i\hat{\phi}^I_{Ii}\mathbf{u}_I + \hat{h}_i\hat{\phi}^I_{Li}\mathbf{u}_L + \hat{h}_i\hat{\phi}^I_{Mi}\mathbf{u}_M\right) \\ & + h_L\left(\hat{h}_i\hat{\phi}^L_{Ii}\mathbf{u}_I + \hat{h}_i\hat{\phi}^L_{Li}\mathbf{u}_L + \hat{h}_i\hat{\phi}^L_{Mi}\mathbf{u}_M\right) \\ & + h_M\left(\hat{h}_i\hat{\phi}^M_{Ii}\mathbf{u}_I + \hat{h}_i\hat{\phi}^M_{Li}\mathbf{u}_L + \hat{h}_i\hat{\phi}^M_{Mi}\mathbf{u}_M\right) \end{aligned} \tag{11}$$

where the term in the parenthesis multiplying h_I gives all the "disk (or

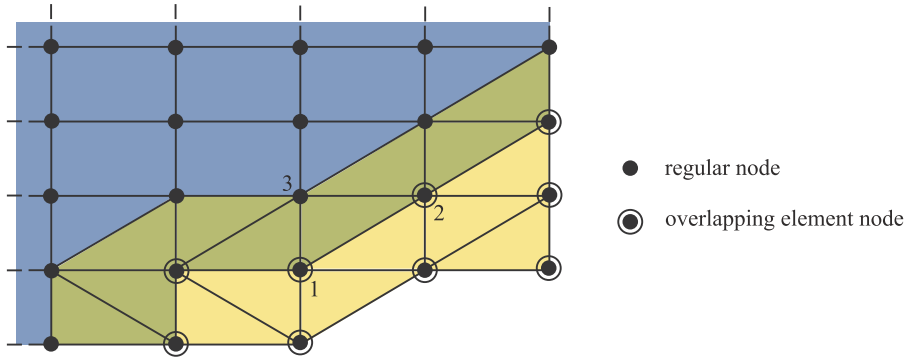

Fig. 10. Coupling region; 3-node and 4-node regular elements (in blue, the element only has regular finite element nodes), 3-node coupling elements (in green, the element has at least one overlapping element node), 3-node overlap elements (in yellow, the element has only overlapping element nodes).

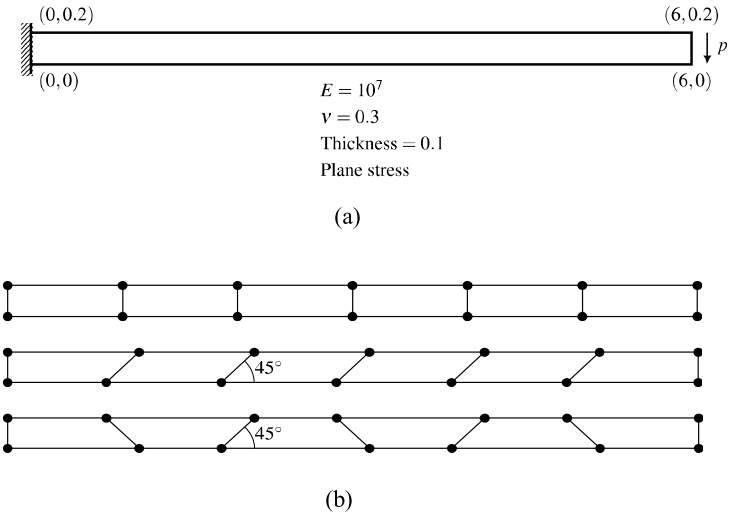

Fig. 11. Analysis of a cantilever; (a) beam problem considered, with traction p, total applied force = 1; (b) meshes used (1 × 6 element meshes); the refined meshes are obtained by subdividing the side lengths of the elements into equal lengths.

Table 2
Calculated tip deflections in beam problem using 4-node elements, the beam reference solution including shear deformations is 0.1081. The number of degrees-of-freedom (dofs) used is given in parentheses. The radii of the disks were chosen to just contain the polygonal element.

	1 × 6 Mesh	3 × 18 Mesh	4 × 24 Mesh
Quadratic overlapping element			
Rectangular	0.1065 (156 dofs)	–	–
Parallelogram	0.1060 (156 dofs)	–	–
Trapezoidal	0.1057 (156 dofs)	–	–
Incompatible modes element [1]			
Rectangular	0.1073 (24 dofs)	0.1076 (144 dofs)	0.1077 (240 dofs)
Parallelogram	0.0675 (24 dofs)	0.1056 (144 dofs)	0.1072 (240 dofs)
Trapezoidal	0.0049 (24 dofs)	0.0964 (144 dofs)	0.1044 (240 dofs)
Traditional 4-node element			
Rectangular	0.0101 (24 dofs)	–	0.0671 (240 dofs)
Parallelogram	0.0037 (24 dofs)	–	0.0395 (240 dofs)
Trapezoidal	0.0029 (24 dofs)	–	0.0502 (240 dofs)

sphere) contributions" from nodes *I, L, M* with the degrees of freedom at these nodes, and similarly for the interpolation functions h_L and h_M.

Considering this equation, we can now see that the complete interpolation can be written in terms of the degrees of freedom at each of the three nodes *I, L, M* as

$$\mathbf{u}(\mathbf{x}) = \rho_I \mathbf{u}_I + \rho_L \mathbf{u}_L + \rho_M \mathbf{u}_M \tag{12}$$

and comparing the above equations we have

$$\begin{aligned} \rho_I &= h_I \hat{h}_i \hat{\phi}^I_{Ii} + h_L \hat{h}_i \hat{\phi}^L_{Ii} + h_M \hat{h}_i \hat{\phi}^M_{Ii} \\ \rho_L &= h_I \hat{h}_i \hat{\phi}^I_{Li} + h_L \hat{h}_i \hat{\phi}^L_{Li} + h_M \hat{h}_i \hat{\phi}^M_{Li} \\ \rho_M &= h_I \hat{h}_i \hat{\phi}^I_{Mi} + h_L \hat{h}_i \hat{\phi}^L_{Mi} + h_M \hat{h}_i \hat{\phi}^M_{Mi} \end{aligned} \tag{13}$$

where we note that ρ_I only involves the disk (or sphere) at node *I*, as is necessary because only the degrees of freedom at node *I* are considered, and similarly for ρ_L and ρ_M. However, the interpolation function corresponding to node *I*, ρ_I, has contributions from the standard h_I with a weight obtained by the disk at node *I*, and has in addition contributions from the other two interpolation functions, h_L and h_M with weights obtained from the disk at node *I* but evaluated for nodes *L* and *M* (for $\psi_L$and ψ_M, respectively).

Hence, we can give the following summary observations regarding the interpolation functions in Eq. (12).

- Firstly, the sum of the interpolations $\hat{h}_i \hat{\phi}^I_{Ni}$, summing over $N = I, L, M$ is equal to 1. The same holds when *I* is replaced by *L* and *M*, see Table 1. Thus the 3-node element satisfies the rigid body mode criterion. The element also passes the patch tests given that the nodal degrees of freedom contain the linear polynomial terms.
- Secondly, since ρ_I is given by h_I times a factor and h_L and h_M times their factors we expect the element behavior to be quite robust with respect to element geometric distortions. In addition, the degrees of freedom given by polynomials at each of the three element nodes render the element distortion-insensitive.

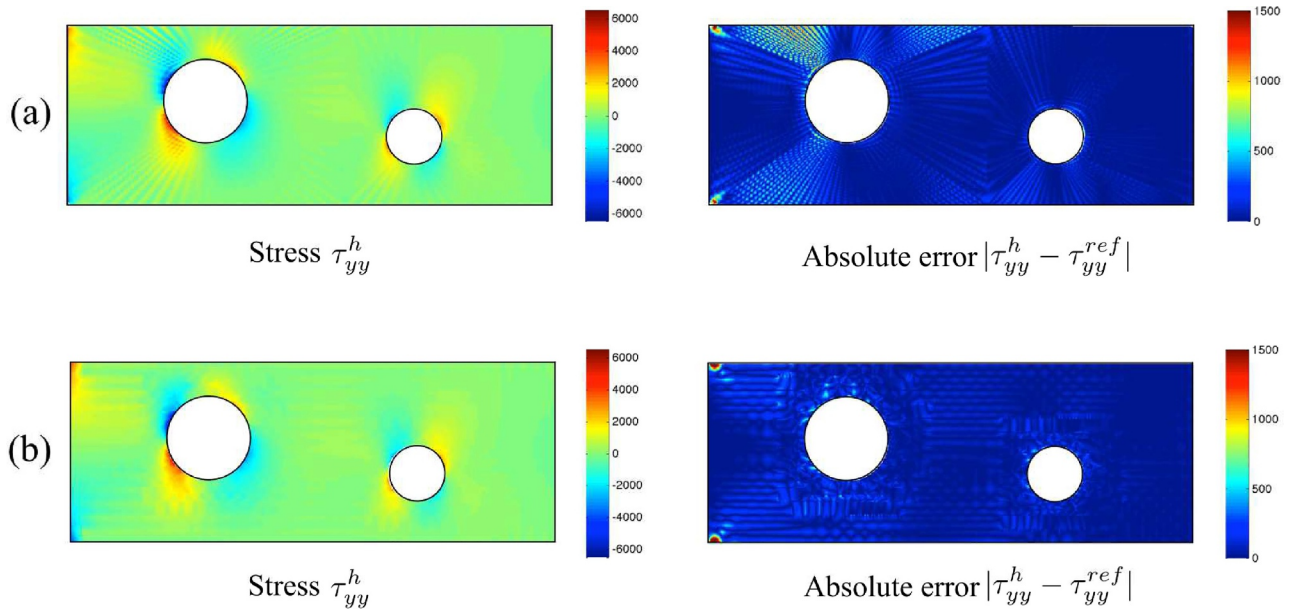

Fig. 12. Stress τ_{yy}^h and absolute error $|\tau_{yy}^h - \tau_{yy}^{ref}|$; (a) 4-node regular finite elements, 4,986 degrees of freedom; (b) solution using AMORE scheme, 2032 degrees of freedom.

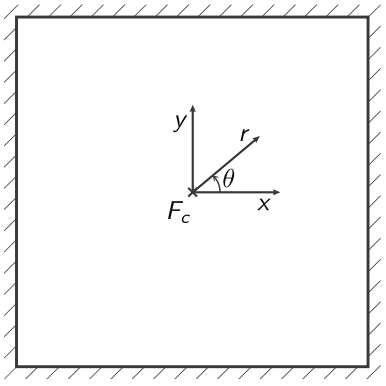

$c = 1$ m/s
$u(\mathbf{x}, t = 0) = 0$ m
$\dot{u}(\mathbf{x}, t = 0) = 0$ m/s

Fig. 13. Pre-stressed membrane considered for wave propagation analysis; a Ricker wavelet point load is applied at the center.

- Thirdly, as the radii r_J of the interpolated Shepard functions increase (or α in Eq. (10) increases) ρ_I approaches h_I. Hence the interpolation scheme reduces to the method using covers [21] and if in addition the polynomial terms p_n in Eq. (3) only consist of the constant term, the scheme reduces to the traditional finite element interpolations. However, for the complete mesh to reduce to the traditional finite element discretization, also the interpolations and degrees of freedom at the boundaries need to do so.

3.1.2. Quadrilateral elements by the overlapping of polygonal elements

Quadrilateral overlapped regions or elements can be formulated in a similar manner as the triangular elements [16].

Referring to Fig. 9 we see that four 9-noded polygonal elements, made each up of four 4-node elements, overlap on the element *I-J-L-M*. To establish the interpolation functions for this element we proceed as for the triangular case.

We also use disks (with Shepard functions) centered at each node to establish the weight functions ϕ_J^I, with *I* and *J* now for all 4 nodes of the element. We interpolate the Shepard functions using the traditional interpolation functions of the 8-node element and can thus construct tables equivalent to Table 1, and establish the interpolation functions ρ_I, ρ_J, ρ_L, ρ_M to obtain [16]

$$\mathbf{u}(\mathbf{x}) = \rho_I \mathbf{u}_I + \rho_J \mathbf{u}_J + \rho_L \mathbf{u}_L + \rho_M \mathbf{u}_M \tag{14}$$

The same observations hold for the quadrilateral element as for the 3-node element discussed above.

3.2. The coupling to regular (traditional) elements

An important ingredient of the AMORE paradigm is the coupling of the regular and overlapping elements. The interpolation functions for the coupling elements are obtained using the above concepts.

Considering an element that couples regular and overlapping finite elements, such as the element with nodes 1,2,3 in the coupling region of Fig. 10, the displacements are given as

$$\mathbf{u}(\mathbf{x}) = \sum_I h_I \boldsymbol{\alpha} + \sum_N h_N \left(\sum_K \phi_K^N \mathbf{u}_K + \sum_J \phi_J^N \boldsymbol{\alpha} \right) \tag{15}$$

with

$$\boldsymbol{\alpha} = \sum_J h_J \mathbf{u}_J + \sum_K h_K \mathbf{a}_{K1} \tag{16}$$

where we now use the subscripts to indicate a summation, *I* and *J* sum over all "usual" finite element nodes of the element (nodes with only the traditional finite element degrees of freedom in $\mathbf{u}_J$), the h_M with any *M* is a regular shape function of the traditional 3-node element, *N* and *K* sum over all nodes of the element that couple into overlapping elements (nodes with polynomials as degrees of freedom in $\mathbf{u}_K$), and we have (since Eq. (4) holds)

$$\sum_K \phi_K^N + \sum_J \phi_J^N = 1 \tag{17}$$

Also $\mathbf{a}_{K1}$ is the solution vector of node *K* corresponding to only the first entries in $\mathbf{u}_K$ (these are the traditional finite element degrees of freedom) . Of course, the ϕ_L^M for any *M, L* are interpolated as in Eq. (4).

The above equations are applicable to triangular and quadrilateral elements. For example, for the coupling element shown in Fig. 10, we have $I = 3$, $J = 3$, $K = 1,2$ and $N = 1,2$ and we note that node 3 has only the usual degrees of freedom whereas nodes 1 and 2 have the degrees of freedom with polynomials. Fig. 10 also illustrates that any node to which a regular element is attached is a "regular node" and is only assigned the regular degrees of freedom. The other nodes are "overlapping element nodes" and have polynomials as degrees of

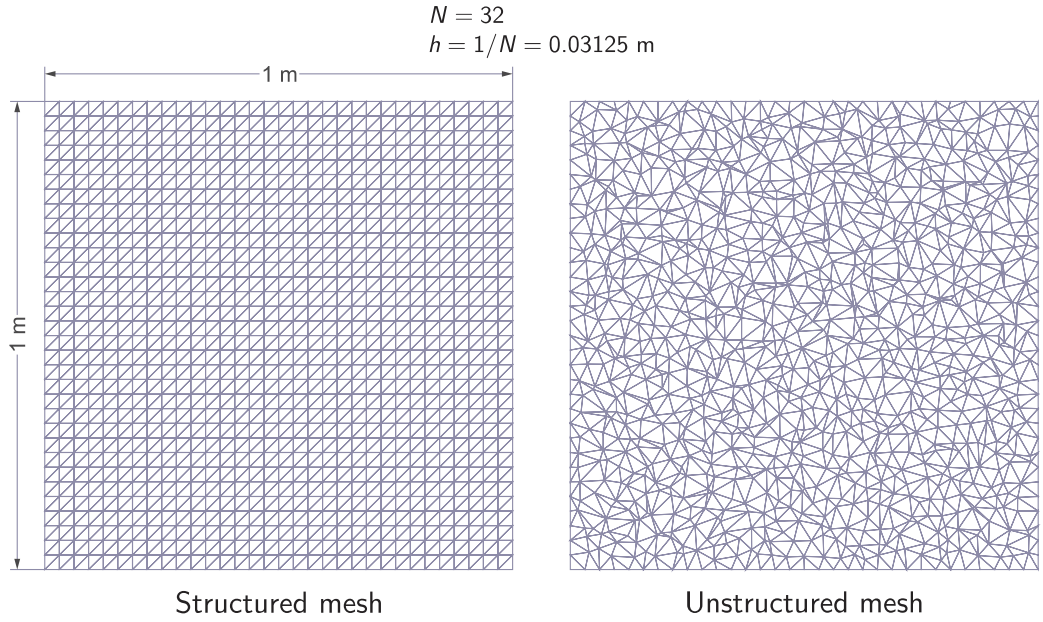

Fig. 14. Meshes used for analysis of pre-stressed membrane; because of symmetry only one quarter of the structure is considered.

freedom.

We note that with this interpolation we also have corresponding to this region a small bandwidth coupling nodes.

To show that with this interpolation the rigid body mode criterion and patch tests are satisfied we see from Eqs. (15) and (16) that for the triangular element (assuming p_n in Eq. (2b) contains the linear terms)

$$\mathbf{u}(\mathbf{x}) = \sum_I h_I \times (linear\ terms) + \sum_N h_N \times (linear\ terms) \tag{18}$$

where we used Eq. (17) (see Table 1). Since also $\sum_I h_I + \sum_N h_N = 1$ we realize that the displacement interpolation contains the linear terms irrespective of any (reasonable) element geometric distortion.

Whenever an element with a regular node has at least one node of an overlapping element (that is, at least one node with the degrees of freedom of a polynomial), the element is a coupling element. Considering the case of an element with no regular finite element node, that is, an element that does not couple into a regular finite element, the summations involving I and J in Eq. (15) are not included and the interpolation reduces to Eq. (11) and hence Eq. (12). On the other hand, if we consider an element that does not couple into an overlapping element, the summations involving N and K in Eqs. (15) and (16) are not included and the equations reduce to the interpolation of the traditional 3-node element.

3.3. Displacement and force boundary conditions

The force (natural) boundary conditions are imposed as usual in finite element analysis, that is, the applied concentrated forces and tractions are taken into the right-hand side load vector of the governing finite element equations [1].

However, some simple special considerations are needed for the displacement (essential) boundary conditions. A direct way to proceed is to use the approach in the finite element method with interpolation covers [21]. For a node J on the boundary with displacement boundary conditions, we simply align the coordinate axes with the tangential and normal directions to the boundary and appropriately impose in $\mathbf{u}_J$ the boundary condition. Hence if, for example, the displacement in the tangential direction is zero, then only the contributions corresponding to the normal direction would be used and be free in $\mathbf{u}_J$.

4. Illustrative analyses

In our research we tested the scheme in 2D analyses for its effectiveness in establishing the governing equations and their solution, and found that the scheme is quite effective regarding the accuracy reached for a reasonable computational effort. Of course, the meshing effort is much reduced. Only preliminary studies of 3D analyses are given in Ref. [14], but based on the 2D and 3D solutions obtained we expect that the procedure is also effective in 3D analyses.

We should recall that the interpolations only involve polynomials and hence the required numerical integrations to obtain the governing matrices only involve a small fraction of the computational effort used in solving the finite element equations, see Ref. [14].

4.1. Static solutions

We consider the cantilever problem with the meshes given in Fig. 11. The problem was proposed in Ref. [22]. The results in Table 2 show that the new quadrilateral element is quite effective, even when the trapezoidal elements are used. Since the element is displacement-based, some locking needs to be expected when the beam is thin, and the MITC procedure might be used to improve the element for such analyses.

Additional solutions for testing the elements discussed above, including convergence studies, are given in Refs. [12–14,16].

To illustrate the AMORE scheme, we solve the cantilever problem mentioned in Section 2 and described in Figs. 3–5. Fig. 12 shows some stress results obtained including a comparison with the results calculated using a rather fine mesh of 4-node traditional elements. We see that although the AMORE mesh is coarser (note the difference in the number of degrees of freedom), smoother stress results are obtained. The efforts to establish and solve the governing equations using the AMORE scheme are about the same as in the traditional finite element solution [14].

4.2. Wave propagation solutions

The accurate analysis of wave propagation problems presents significant difficulties. The numerical dispersion (period elongation) and attenuation (amplitude decay) errors can be severe due to the mesh and time integration scheme used. The time step size Δt for a "given element

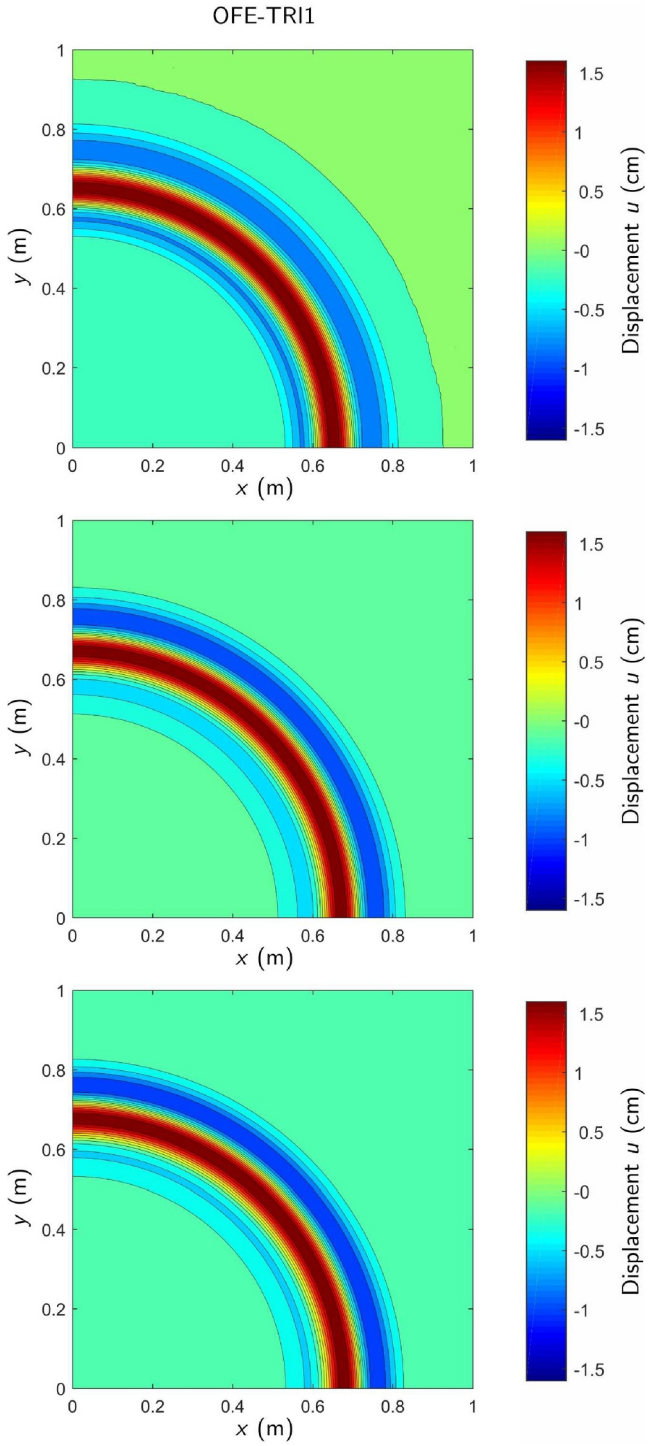

Fig. 15. Contour plots of displacement distributions of the membrane at $t = 0.95s$ calculated using the structured mesh ($h = 0.03125m$) when CFL = 0.5, 0.25, 0.125.

size Δx" is usually selected considering the CFL number

$$CFL = c\Delta t/\Delta x \tag{19}$$

where c is the (analytical) wave speed. The mathematical analysis of a 1D wave propagation problem shows that, for explicit and implicit direct integration schemes, there is an optimal CFL number for which the error of solution is minimum. For a smaller CFL number the use of an explicit or implicit scheme gives larger errors and for a larger CFL number an explicit scheme is usually unstable whereas the use of an implicit scheme gives larger errors. In the analyses of 2D or 3D problems, the meshes need to be uniform and yet numerical dispersion and attenuation errors occur because the "effective element size" varies with the direction considered in the mesh. Furthermore, since the wave speed affects the CFL number, problems containing different waves and velocities are difficult to solve accurately using traditional finite elements.

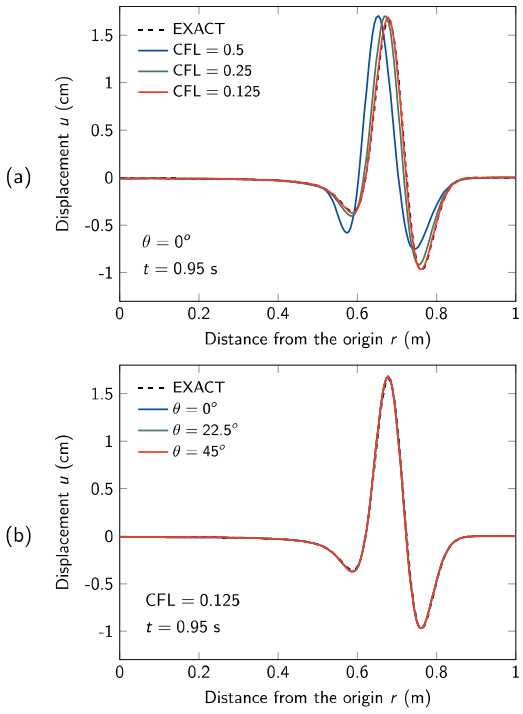

Fig. 16. Displacement distributions of the membrane at $t = 0.95s$ calculated using the unstructured mesh ($h = 0.03125m$); (a) along horizontal axis with decreasing CFL number; (b) along various directions when CFL = 0.125.

We found that the use of overlapping finite elements is providing a valuable avenue to reach better solution accuracy. For wave propagation solutions, we use only overlapping finite elements in the mesh and introduce in addition to the usual polynomial terms in Eq. (3) also degrees of freedom corresponding to trigonometric functions [15,23].

The solution of a prestressed membrane subjected to a point load at its center is addressed in Figs. 13 to 16, where it is seen that excellent results are obtained [15]. For this solution we employed a structured mesh and an unstructured mesh, see Fig. 14. In the interpolations, Eqs. (2) and (3), sine and cosine functions with one wave length over twice the element size h, defined in Fig. 14, are embedded. The element is labeled as OFE-TRI1, and for the time integration the Bathe implicit scheme has been used [1].

Figs. 17 and 18 show an additional solution of a prestressed membrane with holes. For this analysis, we use the AMORE scheme and because of symmetry, only one quarter of the domain (as for the membrane problem above) needs to be considered in the analysis. Good analysis results have been obtained [15].

The important findings are that with a *decrease* of the CFL number the solution results improve and the accuracy of solutions is almost the same in any direction of the (reasonable) meshes used, even when distorted elements are employed. Table 3 gives the computational effort which is also quite reasonable, see Refs. [14,15]. The solution times are clearly small, but unfortunately no comparison with the traditional finite element method is given because whatever reasonable mesh we use, the solution errors with the traditional finite element schemes are too large. These solution times should not be used for a comparison.

Additional numerical solutions are given in Ref. [15]. These excellent solution qualities for a reasonable computational effort are not

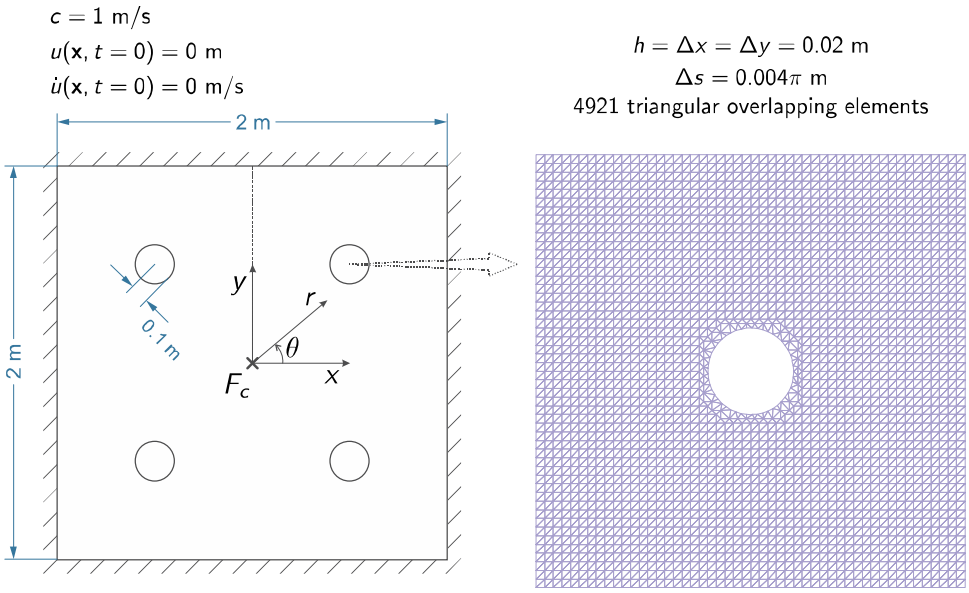

Fig. 17. 2D scalar wave propagation in a pre-stressed membrane with holes; problem description and the mesh used; a Ricker wavelet point load is applied at the center.

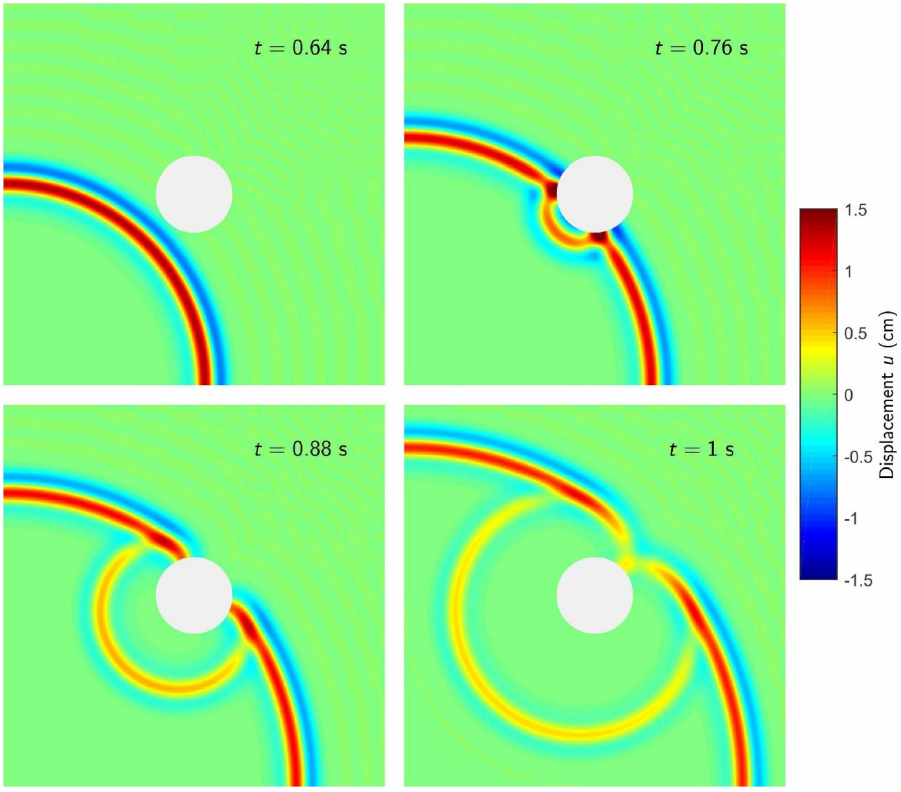

Fig. 18. Snapshots of displacement distributions of the membrane with circular holes at various observation times calculated using the OFE-TRI1 scheme; CFL = 0.125.

seen using traditional finite elements [15,23] or finite spheres [24] when these are supplemented with degrees of freedom for the trigonometric functions.

5. Observations and perspectives

Considering the AMORE paradigm we can identify some important attributes and challenges.

The meshing, see Section 2 and Figs. 1 and 2, can be automatically carried out in a fast computational process. Indeed, the scheme lends itself to be used by a designer and hence there is the potential that the analysis process is moved into design environments.

This attribute is deemed to be a major step towards more use of finite element analysis in early design considerations and structural optimizations in a design process. A designer may run the analysis software used simultaneously on multiple computers and perform optimizations of the design using detailed finite element analysis results.

The basic reason why the meshing is effective is that we couple

Table 3
CPU times used to solve the two-dimensional example problems when using OFE-TRI1 scheme with CFL = 0.125; a 1-core laptop machine is used.

Problem	Number of degrees of freedom	Mean half-bandwidth	CPU time (s) for constructing stiffness and mass matrices	CPU times (s) in the Bathe time integration		
				For initial calculations	For calculations in each time step (Number of time steps)	For total calculation
Membrane	13,068	412	0.3	6.6	0.1 (243)	33.6
Membrane with holes	31,020	844	0.6	73.8	0.5 (400)	274.4

undistorted regular elements in uniform meshes, easily specified, with overlapping elements that are only generated where needed. The regular elements perform well because they are geometrically undistorted and the overlapping elements, while quite distorted, perform well because they are distortion-insensitive.

The fact that the overlapping elements are distortion-insensitive may also be important in dynamic analyses, notably, in the solution of wave propagations, to obtain improved solutions. We obtained encouraging results but further studies are needed.

Specific CAD functions are not used in the finite element formulation and hence, in principle, the AMORE scheme can be used to analyze geometries in whichever way these have been digitized. This aspect should be further explored in research.

While we focused here on the solution of 2D problems in the linear analyses of solids, the avenue of analysis is also promising for the linear analysis of shells and 3D solids, and for nonlinear analyses—but significant research is still required to fully exploit the potential of the AMORE paradigm.

The concepts presented above are directly applicable, but we need to study the locking behavior in the analyses of plates and shells and in the analyses of incompressible media. It will be valuable to identify whether and in how far mixed interpolation is needed in the formulation of overlapping elements.

For the 3D analyses of solids, the convergence behavior and computational efficiency using various overlapping elements needs to be established in depth.

In large deformation analyses, the geometry of the elements can change significantly in certain regions of the domain, and the use of overlapping elements in such regions could be effective.

Considering the analysis of contact problems, in static and dynamic solutions, the use of overlapping elements may be effective but research is needed to establish the effect of the new interpolation functions. A particular attractive feature is that the overlapping elements need not be used to discretize the complete domain of analysis; traditional elements may be used in contact regions.

Furthermore, it would be valuable to study whether and in how much the AMORE paradigm could enhance the meshing and computational schemes for the solutions of fluid flow, electro-magnetic and multi-physics problems.

For all these analysis cases, it would be most valuable to pursue mathematical analyses to obtain deeper insights regarding the discretizations used. Considering applications in engineering practice, also an efficient workflow must be established when complex geometries of multiple parts shall be analyzed using the AMORE scheme.

6. Concluding remarks

We reviewed in this paper the AMORE paradigm and the current state in our developments of overlapping finite elements.

The key to the success of the AMORE paradigm is the use of overlapping elements. Ideally, “general” spheres (disks in 2D analyses) and brick elements (quadrilateral elements in 2D analyses) would be available as overlapping elements, like displayed in Fig. 1. However, to achieve such generality more research is needed.

Therefore, to reach already a practical procedure, we have focused on using the concepts of the method of finite spheres together with traditional finite element interpolations to develop new 3-node and 4-node elements for 2D analyses. These elements are a result of the overlapping of polygonal elements. The same procedure can also be used to formulate 3D elements. We aimed to give the formulations in a transparent manner with novel insight.

While we focused in this paper on the use of AMORE in the CAD process, the scheme is equally applicable to the finite element analysis of 3D computerized scans like used in the medical and building industries, and in terrestrial scanning, see for example Refs. [25,26]. The reason for this direct applicability of AMORE is that specific CAD functions are not used in the finite element formulation, the geometry can be given in various ways, and regular and overlapping elements are used for a finite element analysis.

Based on our experience in the use of AMORE, we can conjecture that there is great potential for use of the AMORE paradigm in practically all areas of finite element analyses. However, much research needs to still be undertaken to fully harvest the full potential of the AMORE scheme.

References

[1] Bathe KJ. Finite element procedures. Prentice Hall, 1996; 2nd ed., Bathe KJ, Watertown, MA, 2014; also published by Higher Education Press China, 2016.
[2] Yu JQ, Cha JZ, Lu YP, Xu WS, Sobolewski M. A CAE-integrated distributed collaborative design system for finite element analysis of complex product based on SOOA. Adv Eng Softw 2010;41:590–603.
[3] Geuzaine C, Remacle JF. Gmsh: a three-dimensional finite element mesh generator with built-in pre- and post-processing facilities. Int. J. Numer. Methods Eng. 2009;79:1309–31.
[4] Nguyen VP, Rabczuk T, Bordas S, Duflot M. Meshless methods: a review and computer implementation aspects. Math Comput Simul 2008;79:763–813.
[5] De S, Bathe KJ. Towards an efficient meshless computational technique: the method of finite spheres. Eng Comput 2001;18:170–92.
[6] Liu GR. Meshfree methods: moving beyond the finite element method. Taylor & Francis; 2009.
[7] Nicomedes WL, Bathe KJ, Moreira FJS, Mesquita RC. Meshfree analysis of electromagnetic wave scattering from conducting targets: formulation and computations. Comput Struct 2017;184:36–52.
[8] Hughes TJR, Cottrell JA, Bazilevs Y. Isogeometric analysis: CAD, finite elements, NURBS, exact geometry and mesh refinement. Comput Methods Appl Mech Eng 2005;194:4135–95.
[9] Bazilevs Y, Calo VM, Hughes TJR, Zhang Y. Isogeometric fluid-structure interaction: theory, algorithms, and computations. Comp Mech 2008;43:3–37.
[10] Kiendl J, Marino E, De Lorenzis L. Isogeometric collocation for the Reissner-Mindlin shell problem. Comput Methods Appl Mech Eng 2017;325:645–65.
[11] Bathe KJ. The finite element method with 'overlapping finite elements' editor In: Zingoni A, editor. Proceedings sixth international conference on structural engineering, mechanics and computation – SEMC 2016South Africa: Cape Town; 2016.
[12] Bathe KJ, Zhang L. The finite element method with overlapping elements – a new paradigm for CAD driven simulations. Comput Struct 2017;182:526–39.
[13] Zhang L, Bathe KJ. Overlapping finite elements for a new paradigm of solution. Comput Struct 2017;187:64–76.
[14] Zhang L, Kim KT, Bathe KJ. The new paradigm of finite element solutions with overlapping elements in CAD – computational efficiency of the procedure. Comput Struct 2018;199:1–17.
[15] Kim KT, Zhang L, Bathe KJ. Transient implicit wave propagation dynamics with overlapping finite elements. Comput Struct 2018;199:18–33.
[16] Huang J, Bathe KJ. Quadrilateral overlapping elements and their use in the AMORE paradigm. In preparation.
[17] Starius G. Composite mesh difference methods for elliptic boundary value problems. Numer Math 1977;28:243–58.
[18] Steger JL, Dougherty FC, Benek JA. A chimera grid scheme. In: Ghia KN, Ghia U, editors. Advances in grid generation, 5. ASME FED; 1983.

[19] Henshaw WD. A high-order accurate parallel solver for Maxwell's equations on overlapping grids. SIAM J. Sci Comput 2006;28:1730–65.
[20] Chan WM. Overset grid technology development at NASA Ames Research Center. Comput Fluids 2009;38:496–503.
[21] Kim J, Bathe KJ. The finite element method enriched by interpolation covers. Comput Struct 2013;116:35–49.
[22] MacNeal RH. A theorem regarding the locking of tapered four-node membrane elements. Int. J. Numer Method Eng 1987;24:1793–9.
[23] Ham S, Bathe KJ. A finite element method enriched for wave propagation problems. Comput Struct 2012;94-95:1–12.
[24] Ham S, Lai B, Bathe KJ. The method of finite spheres for wave propagation problems. Comput Struct 2014;142:1–14.
[25] Farahani N, Braun A, Jutt D, Huffman T, Reder N, Liu Z, Yagi Y, Pantanowitz L. Three-dimensional imaging and scanning: current and future applications for pathology. J Pathol Inform 2017;8:36.
[26] Axelsson P. Processing of laser scanner data – algorithms and applications. J Photogrammetry and Remote Sens 1999;54:138–47.